Excess equimolar radius of liquid drops

Martin Horsch* and Hans Hasse
Lehrstuhl für Thermodynamik, Fachbereich Maschinenbau und Verfahrenstechnik, Technische Universität Kaiserslautern, Erwin-Schrödinger-Str. 44, 67663 Kaiserslautern, Germany

Alexander K. Shchekin
Department of Statistical Physics, Faculty of Physics, Saint Petersburg State University, ulica Ulyanovskaya, Petrodvoretz, 198504 Saint Petersburg, Russia

Animesh Agarwal, Stefan Eckelsbach, and Jadran Vrabec
Lehrstuhl für Thermodynamik und Energietechnik, Institut für Verfahrenstechnik, Universität Paderborn, Warburger Str. 100, 33098 Paderborn, Germany

Erich A. Müller and George Jackson
Molecular Systems Engineering Group, Department of Chemical Engineering, Imperial College London, London SW7 2AZ, United Kingdom
(Received 26 September 2011; published 26 March 2012)

The curvature dependence of the surface tension is related to the excess equimolar radius of liquid drops, i.e., the deviation of the equimolar radius from the radius defined by the macroscopic capillarity approximation. Based on the Tolman [J. Chem. Phys. **17**, 333 (1949)] approach and its interpretation by Nijmeijer *et al.* [J. Chem. Phys. **96**, 565 (1991)], the surface tension of spherical interfaces is analyzed in terms of the pressure difference due to curvature. In the present study, the excess equimolar radius, which can be obtained directly from the density profile, is used instead of the Tolman length. Liquid drops of the truncated and shifted Lennard-Jones fluid are investigated by molecular dynamics simulation in the canonical ensemble, with equimolar radii ranging from 4 to 33 times the Lennard-Jones size parameter σ. In these simulations, the magnitude of the excess equimolar radius is shown to be smaller than $\sigma/2$. This suggests that the surface tension of liquid drops at the nanometer length scale is much closer to that of the planar vapor-liquid interface than reported in studies based on the mechanical route.

DOI: 10.1103/PhysRevE.85.031605 PACS number(s): 68.03.Cd, 05.70.Np, 05.20.Jj

I. INTRODUCTION

The macroscopic capillarity approximation consists in neglecting the curvature dependence of the surface tension γ of a spherical liquid drop. Accordingly, the surface tension of a curved interface in equilibrium is approximated by its value γ_∞ in the zero-curvature limit, i.e., for a planar vapor-liquid interface. The Young-Laplace equation [1–3] for spherical interfaces relates the macroscopic surface tension to a characteristic radius of the liquid drop,

$$R_\kappa = \frac{2\gamma_\infty}{P^\ell - P^v} = \frac{\gamma_\infty}{\varphi}, \tag{1}$$

which will be referred to as the capillarity radius here; the notation $\varphi = (P^\ell - P^v)/2$ for half of the difference between the liquid pressure P^ℓ and the vapor pressure P^v is introduced for convenience. At equilibrium, the temperature is the same for both phases, and the pressures P^ℓ and P^v correspond to states with the same chemical potential. Both the drop radius and the pressure difference characterize the extent by which the surface is curved. The surface tension γ_∞ of the planar vapor-liquid phase boundary, which is relatively easy to access experimentally, couples $1/R_\kappa$ and φ, i.e., two measures of curvature, as a proportionality constant.

For curved interfaces in equilibrium, the chemical potential μ deviates from its saturation value μ_s for a flat interface. The precise conditions can be determined from the pressure difference between the fluid phases by means of an equation of state. In the case of a drop, both phases are supersaturated. To realize this, it is sufficient to consider the Gibbs-Duhem equation for a curved phase boundary.[1] Since the chemical potential must be equal for all phases in (stable or unstable) equilibrium, one obtains

$$d(P^\ell - P^v) = (\rho^\ell - \rho^v)d\mu. \tag{2}$$

For a planar interface, both phases coexist at the saturation condition ($\mu = \mu_s$) and the pressure difference is zero. The number density of the liquid phase ρ^ℓ is larger than that of the vapor ρ^v, so that raising the value of the liquid pressure P^ℓ over the vapor pressure P^v increases the chemical potential μ. Therefore, its value for a system comprising a liquid drop, where P^ℓ is greater than P^v, has to exceed μ_s.

In combination with an equation of state for the bulk fluid, microscopic properties such as the radius of a small liquid drop can thus be deduced from the macroscopic state of the surrounding vapor, i.e., from its supersaturation ratio, and vice

*Corresponding author: Also at Imperial College, London, UK; martin.horsch@mv.uni-kl.de

[1] In the following discussion, the temperature T is treated as a parameter (rather than a variable), so that total differentials are to be understood as partial derivatives at constant temperature.

versa. This approach is the most widespread interpretation of the Gibbs theory of interfaces [4,5], and it is the point of departure for classical nucleation theory as introduced by Volmer and Weber [6] and further developed by Farkas [7] as well as subsequent authors [8–10]. The Gibbs approach presupposes a sharp dividing surface between the phases, a conceptual picture that does not reflect the physical features at the molecular length scale. However, this abstraction is precisely its strength. Instead of discussing thermodynamic properties such as the density, the pressure tensor, and the free-energy density in a localized way, interfacial excess quantities can be assigned to the formal dividing surface as a whole.

Significant size effects on interfacial properties had already been detected experimentally by Weber [11] at the turn of the century. These were also known to Farkas [7], who stated explicitly that the capillarity approximation should be expected to fail for radii at the length scale of the intermolecular interactions. In the absence of a better approximation, however, the surface tension of the planar phase boundary had to be used as input for nucleation theory, and little has changed in this respect in the meantime.

In the case of significant deviations from the macroscopic capillarity approximation, liquid drops cannot be characterized sufficiently by a single effective radius. Instead, the capillarity radius R_κ is distinct from the equimolar radius R_ρ, which is also known as the Gibbs adsorption radius. For a single-component system, the latter is defined by the zero-excess-density criterion

$$\int_0^{R_\rho} dz\, z^2[\rho(z)-\rho^\ell(\mu,T)]+\int_{R_\rho}^{\infty} dz\, z^2[\rho(z)-\rho^v(\mu,T)]=0, \tag{3}$$

where one compares a step function using the bulk liquid and vapor number densities (as functions of μ and T) with the microscopic radial density profile $\rho(z)$. By convention, the density ρ corresponds to the number of particles per unit volume here, rather than their mass, and z denotes the distance from the center of mass of the liquid drop.

In addition to R_κ and R_ρ, a thermodynamically relevant definition of the liquid drop size is given by the surface of tension radius

$$R_\gamma = \frac{\gamma}{\varphi}, \tag{4}$$

which is also known as the Laplace radius. It can be obtained by inserting the actual value of the surface tension γ of the system with the curved interface (not the planar limit value γ_∞) into the Young-Laplace equation. This radius can be related to the surface area a and to the volume V of the drop,

$$R_\gamma\, da = 2\, dV. \tag{5}$$

This relation can be expressed in terms of the excess grand potential Σ of the surface as

$$R_\gamma\, d\Sigma = 2\gamma\, dV, \tag{6}$$

where the surface tension is defined through the formal thermodynamic relation

$$\gamma = \frac{d\Sigma}{da}. \tag{7}$$

Modified versions of the Young-Laplace equation, which allow for the use of different radii in an analogous way, were introduced by Buff [12,13] and Kondo [14].

The present study deals with the deviation between the capillarity radius R_κ, the equimolar radius R_ρ, and the surface of tension radius R_γ of a liquid drop in equilibrium with a supersaturated vapor. As Tolman [15–17], following Gibbs, showed on the basis of axiomatic thermodynamics, one of these differences, now commonly referred to as the Tolman length

$$\delta = R_\rho - R_\gamma, \tag{8}$$

is sufficient to characterize the curvature dependence of the surface tension [17],

$$\frac{d\ln R_\gamma}{d\ln \gamma} = 1+\frac{1}{2}\left(\frac{\delta}{R_\gamma}+\left[\frac{\delta}{R_\gamma}\right]^2+\frac{1}{3}\left[\frac{\delta}{R_\gamma}\right]^3\right)^{-1}. \tag{9}$$

Castellanos *et al.* [18] have conjectured that "the Tolman length is related to the interfacial width Δ^σ according to $\Delta^\sigma \approx 2\delta$." It is important to point out that Eq. (9) follows the approach of Gibbs strictly, i.e., without neglecting any of the higher-order curvature terms. The cubic expression originates from an integral over the spherical density profile.

However, this relation is often transformed into a polynomial expansion for γ_∞/γ, which contains an infinite number of terms and has to be truncated, e.g., after the second-order contribution in terms of curvature [19],

$$\frac{\gamma_\infty}{\gamma} = 1+\frac{2\delta_\infty}{R_\gamma}+2\left(\frac{\lambda}{R_\gamma}\right)^2+O\left(R_\gamma^{-3}\right). \tag{10}$$

Here, δ_∞ is the Tolman length in the limit of an infinite radius (i.e., zero curvature). The length λ characterizes the effect of the Gaussian curvature that becomes predominant when δ is very small or for systems where, due to an inherent symmetry, $\delta = 0$ holds by construction [19,20]; a similar leading term, proportional to $R_\gamma^{-2}\ln R_\gamma$, has also been deduced by Bieker and Dietrich [21] from density functional theory based on a Barker-Henderson perturbation expansion.

One should keep in mind that the Tolman equation as given by Eq. (9) is valid for curved phase boundaries of pure fluids in general, whereas truncated polynomial expansions in terms of the curvature $1/R_\gamma$ like Eq. (10) break down for liquid drops at the molecular length scale. In practice, one of the major problems of the Tolman approach is that it analyzes the surface tension in terms of the radii R_ρ and R_γ (because δ is the difference between the radii). While R_ρ can be immediately obtained from the density profile, R_γ is by definition related to γ itself. Since for highly curved interfaces the value of γ is disputed or unknown [22–24], the surface of tension radius R_γ and its deviation from R_ρ is correspondingly uncertain.

To resolve this issue, we reformulate Tolman's theory in terms of R_κ and R_ρ. This leads to greater transparency, since the capillarity radius R_κ can be obtained on the basis of properties of the (stable and metastable) bulk fluid and the surface tension in the planar limit γ_∞, which is experimentally

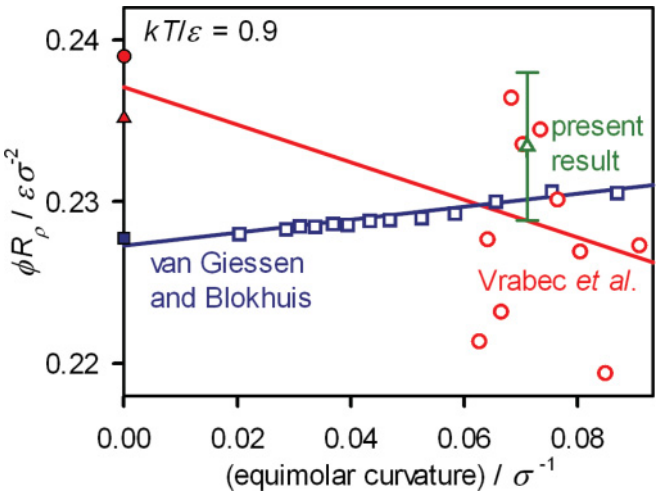

FIG. 1. (Color online) Diagram of van Giessen and Blokhuis [26], showing φR_ρ as a function of the equimolar curvature $1/R_\rho$ for liquid drops of the truncated-shifted Lennard-Jones fluid at a reduced temperature of $kT/\varepsilon = 0.9$, where R_ρ is determined from the density profiles and φ from the difference between the values of the normal component of the Irving-Kirkwood pressure tensor in the homogeneous regions inside the liquid drop as well as outside, i.e., in the homogeneous supersaturated vapor. In addition to the results of van Giessen and Blokhuis (□), the data of Vrabec *et al.* [27] (○), which were obtained using the same method, are included here along with a data point (△) where φ is determined by MD simulation of the homogeneous fluid. The data for the planar surface tension γ_∞ are taken from simulations of Vrabec *et al.* (●) and van Giessen and Blokhuis (■) as well as the correlation of Vrabec *et al.* (▲). The continuous lines are guides to the eye: In the planar limit, a positive slope corresponds to a negative Tolman length and vice versa; cf. Eq. (12).

accessible.[2] All information on the molecular structure of the curved interface can thus be captured by a single undisputed quantity here, namely, the equimolar radius R_ρ. In our approach, the excess equimolar radius, defined as

$$\eta = R_\rho - R_\kappa, \tag{11}$$

plays a role similar to the Tolman length, and the macroscopic quantity φ is used instead of $1/R_\gamma$ as a measure of the influence of curvature on the thermophysical properties of the interface and the bulk phases. In this way, the thermodynamics of liquid drops is discussed by following a different route that relies on the density profiles and bulk properties only, avoiding the intricacies of defining the pressure tensor or the change in the surface area as required by other approaches.

The present method is related to the direct determination of δ_∞ proposed by Nijmeijer *et al.* [25], which was recently implemented by van Giessen and Blokhuis [26] on the basis of a representation of the ratio of φR_ρ to the curvature as defined by $1/R_\rho$ with

$$-\delta_\infty = \frac{1}{\gamma_\infty}\left(\lim_{R_\rho\to\infty}\frac{d}{d(1/R_\rho)}\varphi R_\rho\right), \tag{12}$$

as depicted in Fig. 1. However, the method suggested here differs from that of van Giessen and Blokhuis, which relies on a pressure tensor to obtain φ, whereas in the present work, the pressure difference is determined by molecular dynamics (MD) simulation of the bulk fluids. Applying the definitions of the capillarity radius and the excess equimolar radius, Eq. (12) transforms to

$$-\delta_\infty = \lim_{R_\rho\to\infty}\frac{d(R_\rho/R_\kappa)}{d(1/R_\rho)} = \lim_{R_\rho\to\infty}\frac{d(\eta/R_\kappa)}{d(1/R_\rho)}, \tag{13}$$

facilitating an analysis of the interfacial properties in terms of the radii R_κ and R_ρ as well as the deviation η between them.

This paper is structured as follows: In Sec. II, a review is made of the available routes to the Tolman length and the surface tension by molecular simulation. MD methods directly related to nucleation itself, from which information about the excess free energy of curved interfaces can also be deduced [28–31], are not included in the current discussion; in this regard, the reader is referred to Chkonia *et al.* [32]. Section III is dedicated to a brief outline of how Tolman's thermodynamic approach is transformed by analyzing the surface tension in terms of η and φ rather than δ and $1/R_\gamma$. The methodology and the results of a series of canonical ensemble MD simulations, where the excess equimolar radius is obtained solely on the basis of density profiles, are presented in Sec. IV. An interpretation of these results is given in Sec. V, leading to the conclusion that previous studies relying on a mechanical (i.e., pressure tensor based) route to the surface tension have overestimated the curvature dependence of γ.

II. THE TOLMAN LENGTH FROM MOLECULAR SIMULATION

A. Analysis of the planar interface

For the planar interface, the pressure is equal on both sides of the interface and the surface of tension radius R_γ becomes ill defined [cf. Eq. (4)], so that the definition of the Tolman length given by Eq. (8) ceases to be applicable in the absence of curvature. Therefore, the Tolman length of the planar interface δ_∞ necessarily has to be derived from considerations pertaining to curved geometries. It can be obtained either by extrapolating results for δ to the macroscopic limit $\varphi \to 0$ (i.e., $R_\gamma \to \infty$) or by constructing the limit explicitly from expressions for the radii R_ρ and R_γ. The latter approach was followed by Fisher and Wortis [33] who, on the basis of a Landau (square-gradient) theory, derived the relation

$$-\delta_\infty = \frac{1}{\Delta\rho}\int_{z=-\infty}^{z=\infty} d\rho_\infty(z)\, z + \frac{\int_{z=-\infty}^{z=\infty} d\rho_\infty(z)[d\rho_\infty(z)/d\ln z]}{\int_{z=-\infty}^{z=\infty} d\rho_\infty(z)[d\rho_\infty(z)/dz]}, \tag{14}$$

in terms of the density profile $\rho_\infty(z)$ of the planar interface. This expression can also be extended to account for the pair density profile, whereby Eq. (14) becomes a limiting case [34,35].

The available computational methods for evaluating the Tolman length of curved interfaces, however, involve the determination of the surface tension γ. It is usually the methodology related to the evaluation of γ that is both

[2]The pressure difference between the coexisting phases in equilibrium is a bulk property, since it can be determined from μ and T with an equation of state for the fluid.

the crucial and the most debatable step, which is made evident by the contradictory findings for γ (and consequently also for δ_∞) obtained with different methods. Three routes to the surface tension of liquid drops will now be discussed briefly: the mechanical route as implemented by Thompson *et al.* [36], the grand canonical route of Schrader *et al.* [37], and the free-energy difference route developed by Sampayo *et al.* [23].

Many different versions and combinations of these approaches exist [38–40], but it would be inappropriate to attempt a full appreciation of the complete body of work here. The reader is directed to the excellent review by Henderson [41] for a detailed discussion of the underlying statistical mechanical approaches.

B. The mechanical route

The mechanical route to the surface tension is based on the Bakker-Buff equation for spherical interfaces [13,36,42,43],

$$\gamma = R_\gamma^{-2} \int_{z=0}^{z=\infty} dz\, z^2 [P_n(z) - P_t(z)], \tag{15}$$

in terms of the normal component $P_n(z)$ and the two (equal) tangential components $P_t(z)$ of the diagonalized pressure tensor, which is considered as a spherical average, and where the integration starts from the center of the drop ($z = 0$). With this relation one expresses the work required for a reversible isothermal deformation of the system that leads to an infinitesimal increase of the surface area at constant volume, which coincides with the corresponding free-energy difference. It is sufficient to compute either the normal or the tangential pressure profile, since the two are related by [36,44]

$$\frac{dP_n}{d\ln z} = 2(P_t - P_n). \tag{16}$$

At mechanical equilibrium, Eq. (15) can thus be transformed to [36]

$$2\gamma^3 = -\varphi^2 \int_{z=0}^{z=\infty} dP_n(z)\, z^3, \tag{17}$$

a relation in which R_γ no longer appears. The surface of tension radius R_γ can be obtained from Eq. (4) once the surface tension γ is known.

The most widespread implementation of this approach in terms of intermolecular pair potentials makes use of the Irving-Kirkwood (IK) pressure tensor [45], which was applied to spherical interfaces by Buff [13]. It underlies the simulation studies of Vrabec *et al.* [27] as well as those of van Giessen and Blokhuis [26]. The normal component of the IK pressure tensor is given by [36,45]

$$P_n(z) = kT\rho(z) + \sum_{\{i,j\}\in\mathbf{S}} -\frac{du_{ij}}{dr_{ij}} \frac{|\mathbf{z}\cdot\mathbf{r}_{ij}|}{4\pi z^3 r_{ij}}, \tag{18}$$

where k is the Boltzmann constant and the summation covers the set $\mathbf{S}$ containing all sets of particles i and j connected by a line that intersects the sphere of radius z around the center of mass of the liquid drop. The intersection coordinates (relative to the center of mass) are represented by $\mathbf{z}$ and the distance between the particles by $\mathbf{r}_{ij}$ with $r_{ij} = |\mathbf{r}_{ij}|$, while $-du_{ij}/dr_{ij}$ is the force acting between the two particles i and j.

Regarding the mechanical route as described here, various issues arise:

(a) Irving and Kirkwood [45] originally proposed their expression for the special case of "a single-component, single-phase system." Its derivation relies on truncating an expansion in terms of derivatives of the pair density $\rho^{(2)}$ after the first term, thereby disregarding the density gradient completely. For a liquid drop, this can lead to inaccuracies: "at a boundary or interface ... neglecting terms beyond the first may not be justified" [45]. Nonetheless, Blokhuis and Bedeaux [46] have shown that the IK tensor leads to the correct expression for φ (to third order in terms of the equimolar curvature), and thus to the correct value for δ_∞.

(b) By construction, the mechanical route cannot be separated from the assumption of mechanical equilibrium that underlies the basic approach, i.e., Eqs. (15)–(17). For nanoscopic liquid drops, however, configurations that are not in mechanical equilibrium correspond to a significant fraction of the partition function, and it is not clear to what extent the spherical average of the pressure tensor succeeds in accounting for the free-energy contribution of capillary waves, i.e., the excited vibrational modes of the interface [47,48]. An additional entropic contribution to the surface free energy due to large fluctuations in the energy is responsible for this [23]. For the truncated-shifted Lennard-Jones (TSLJ) fluid, the deviation of the Tolman length resulting from the use of the Bakker-Buff equation is quite significant [49], overestimating the value of δ_∞ obtained with the approach of Blokhuis and Bedeaux [46] by an order of magnitude.

(c) The nonunique nature of the pressure tensor, which for a planar interface does not affect the computed value of the surface tension [50], leads to an inconsistent description for a curved interface [40,41,51]. However, the Harasima pressure tensor [43], where the set $\mathbf{S}$ is defined differently and the tangential pressure profile $P_t(z)$ is computed instead of the normal component $P_n(z)$, has been found to agree rather well with the IK tensor [27,39,50].

C. The grand canonical route

From an analysis of the canonical partition function, Binder [48] has derived very useful scaling laws for the probability $\omega(\rho_{\min})$ that a relatively small subvolume has the density $\rho_{\min}$ corresponding to a maximum of the local free energy, i.e., the least probable local density between ρ^ℓ and ρ^v. It follows that "the probability of a *homogeneous* state with order parameter $\rho_{\min}$ decreases exponentially fast with the volume" while for cases where the corresponding subvolume is situated within a phase boundary the probability "decreases exponentially fast with the interface area" [48]. The surface excess of the grand potential (per unit surface area) can thus be determined as

$$f^E = \lim_{a\to\infty} \frac{\Sigma}{a} = kT \lim_{L\to\infty} \frac{\ln \omega(\rho_{\min})}{a(L)}, \tag{19}$$

which is related to the surface tension by $\gamma = d\Sigma/da$. Therein, the term $a(L)$ describes the dependence of the surface area on the characteristic length L of the system [48], e.g., $a(L) = 2L^2$ for a planar slab in a cubic volume $V = L^3$ with standard periodic boundary conditions.

Small subvolumes of a canonical system in the thermodynamic limit ($N \to \infty$) are equivalent to systems with constant μ, V, and T so that grand canonical Monte Carlo simulation can be applied. Umbrella sampling may be used to fully sample the relevant range of values for the order parameter [52,53], i.e., the number of particles N present in the grand canonical system. Thereby, a profile is obtained for the free-energy density $f(N)$ or, equivalently, $f(\rho)$.

To analyze liquid drops of a certain size, however, the limit $a \to \infty$ cannot be applied since the area a of the surface of tension is fixed. Instead, the surface excess term $f^E(R_\rho)$ is determined from expressions based on the equimolar radius [37],

$$f(\rho) = \frac{V^\ell}{V}\rho^\ell(R_\rho)\mu(R_\rho) + \frac{V^v}{V}\rho^v(R_\rho)\mu(R_\rho) + \frac{4\pi R_\rho^2}{V} f^E(R_\rho). \tag{20}$$

Here, $V^\ell = 4\pi R_\rho^3/3$ is the volume associated with the liquid phase, $V^v = V - V^\ell$ is the remainder of the volume, and $\rho^\ell(R_\rho)$ as well as $\rho^v(R_\rho)$ are bulk densities related to the liquid drop and the surrounding vapor. The chemical potential $\mu(R_\rho)$ is equal for the vapor and liquid regions, but different from both the saturated bulk value μ_s and the chemical potential μ set in the grand canonical simulation itself. This approach has recently been employed to examine the properties of drops, bubbles, and symmetric liquid-liquid interfaces in great detail [19,20,22,37,54].

The original method of Binder [48] was developed for planar interfaces. In the case of systems with a spherical geometry, the following points ought to be kept in mind:

(a) Following the approach of Schrader *et al.* [37], the surface tension γ can be accessed only indirectly, e.g., from Eq. (6), based on the surface of tension radius R_γ, which also has to be obtained in a circuitous manner. Thereby, care should be taken not to confuse f^E with γ, or R_ρ with R_γ [54].

(b) Since the infinite size limit [cf. Eq. (19)] does not apply to nanoscopic liquid drops and the systems under consideration can be extremely small, it is not generally possible to neglect the contribution of homogeneous configurations to $f(\rho)$.

(c) The assumption that $4\pi R_\rho^2$ is the surface area associated with the surface excess for the grand potential of the system, as in Eq. (20), essentially amounts to applying the macroscopic capillarity approximation. Such an approach may be justified under certain circumstances, but for investigations of the *deviation* from capillarity it is of limited use only.

Other umbrella sampling based methods [55,56], which will not be discussed here, are confronted with similar difficulties, in particular regarding the relation between the surface tension and the surface excess free energy.

D. The free-energy difference route

The free-energy difference route to the surface tension is based on Bennett's [57] general considerations of the molecular simulation of free energies and entropic quantities. In the canonical ensemble, the free-energy difference $\Delta A = A_1 - A_0$ between two states with equal N, V, and T is related to the quotient of the respective canonical partition functions Z_0 and Z_1, which can be evaluated from ensemble averages [57]:

$$\exp\left(\frac{\Delta A}{kT}\right) = \frac{Z_0}{Z_1} = \frac{\left\langle \min\left(\exp\left(\frac{\Delta E}{kT}\right),1\right)\right\rangle_1}{\left\langle \min\left(\exp\left(\frac{-\Delta E}{kT}\right),1\right)\right\rangle_0}, \tag{21}$$

in terms of the internal energy difference $\Delta E = E_1 - E_0$. The index of the angular brackets denotes the system over which the ensemble average is taken. Bennett proposed the determination of these energy differences from "separately generated samples" [57] for E_0 and E_1. If the two systems differ in the area of a phase boundary, then the free-energy difference can be related to the surface tension, assuming that all other deviations between them are accurately taken into account.

Gloor *et al.* [38] introduced a version of this approach where differences between the two states are obtained from a single simulation run for an unperturbed system with the partition function Z_0. Corresponding configurations of the second, perturbed system are generated by performing small affine transformations, keeping the volume and the number of particles in both phases constant. In the limit of an infinitesimal distortion of the system, Eq. (21) can be simplified as [38,58]

$$\frac{\Delta A}{kT} = -\ln\left\langle \exp\left(\frac{-\Delta E}{kT}\right)\right\rangle_0, \tag{22}$$

as the probability distribution functions of the ensembles corresponding to the unperturbed and the perturbed systems converge, so that separate sampling is no longer required. A third-order expansion in the inverse temperature [58],

$$\frac{\Delta A}{kT} = \frac{\langle \Delta E\rangle}{kT} - \frac{\langle \Delta E^2\rangle - \langle \Delta E\rangle^2}{2(kT)^2} + \frac{\langle \Delta E^3\rangle - 3\langle \Delta E^2\rangle\langle \Delta E\rangle + 2\langle \Delta E\rangle^3}{6(kT)^3}, \tag{23}$$

can be used to increase the precision of the simulation results [23,38]. The surface tension is then immediately obtained from $\Delta A/\Delta a$, since the distortion of the interface itself (as opposed to its increase in area) makes a negligible contribution to the free-energy difference [15].

In analogy with the Widom test-particle method [59], this implementation of the free-energy difference route is also called the test-area method [38,60]. Following Sampayo *et al.* [23], it can be applied to curved interfaces, where the affine transformation scales one of the Cartesian axes by the factor $1/(1+\xi)$ and the remaining ones by $(1+\xi)^{1/2}$. For $\xi > 0$, this creates an oblate shape and the area of the surface of tension is increased by [61]

$$\frac{\Delta a}{\pi R_\rho^2} = 2(1+\xi) + \frac{\ln([1+\Xi]/[1-\Xi])}{(1+\xi)^2\Xi} + O\left(\frac{\delta\,\Delta a}{R_\rho^3}\right), \tag{24}$$

with the ellipticity of the average equimolar surface in the perturbed system given by $\Xi = [1-(1+\xi)^{-3}]^{1/2}$. In the prolate case ($\xi < 0$), the corresponding term is $\Xi = [1-(1-\xi)^{-3}]^{1/2}$ and the change in area is [61]

$$\frac{\Delta a}{\pi R_\rho^2} = 2\left(\frac{\arcsin\Xi}{\Xi(1-\xi)^{1/2}} - \xi - 1\right) + O\left(\frac{\delta\,\Delta a}{R_\rho^3}\right). \tag{25}$$

It can be shown that the first-order term in Eq. (23) is equivalent to the Kirkwood-Buff [62] mechanical expression for the surface tension [63]. The higher-order terms therefore presumably capture the deviation between the mechanical and free-energy difference routes due to fluctuations or, equivalently, the contribution of configurations which are not in mechanical equilibrium to γ. Thus, the higher-order contribution to Eq. (23) may be related to the closed expression derived by Percus *et al.* [64] for the deviation between the actual free energy and an approximation based on the local pressure.

From this point of view, the following aspects of the method merit further consideration:

(a) While finite differences of higher order are taken into account for the energy, no such terms are considered for the surface area here. Clearly, the variance of ΔE is partly caused by the variance of Δa. The use of R_ρ in the definition of the surface area [cf. Eqs. (24) and (25)] may lead to further deviations.

(b) The variance of ΔE accounts for surface oscillations such as long-wavelength capillary waves, which are directly related to equilibrium properties of the interface and therefore do not depend on the statistical mechanical ensemble [41]. However, it can also be influenced by fluctuations in ρ^ℓ (at constant V^ℓ) or V^ℓ (at constant ρ^ℓ). These modes are ensemble dependent, since they are coupled to the density of the vapor phase. Canonically, their amplitude increases with the total volume and is ill defined in the thermodynamic limit $V \to \infty$. Therefore, the surface tension from the free-energy difference route may depend on the constraints imposed on the system by the ensemble.

(c) Although the volume associated with each of the phases is invariant for test-area transformations, there is still a distortion of the sample with respect to the equilibrium conformation. The method is therefore limited to isotropic phases, since shearing an anisotropic phase will induce an elastic contribution in ΔA from the bulk region as well.

III. TOLMAN'S APPROACH IN TERMS OF THE EXCESS EQUIMOLAR RADIUS

From the Tolman equation in its approximate polynomial form [cf. Eq. (10)], the excess equimolar radius η can be related to the Tolman length δ by

$$\begin{aligned}\eta &= (\delta + R_\gamma) - R_\kappa \\ &= \delta + R_\gamma \left(1 - \left[1 + \frac{2\delta_\infty}{R_\gamma} + O\left(R_\gamma^{-2}\right)\right]\right) \\ &= -\delta + O\left(R_\gamma^{-1}\right),\end{aligned} \tag{26}$$

so that its magnitude in the zero-curvature limit is obtained as

$$\eta_\infty = -\delta_\infty. \tag{27}$$

Essentially, this expresses the same relationship as Eq. (13). Both in the planar limit and in the presence of curvature effects, it is therefore possible to rewrite the Tolman relations in terms of the easily accessible quantities η and φ, rather than δ and $1/R_\gamma$.

The starting point for such an expression is the exact closed form of the Tolman equation [cf. Eq. (9)], which is derived from the Gibbs-Duhem equation, the Young-Laplace equation, and the Gibbs adsorption equation [17]; hence, it is based entirely on an axiomatic thermodynamic treatment. As opposed to truncated power series of the form of Eq. (10), the description given by Eq. (9) remains valid when the radius R_γ becomes similar to or smaller than $|\delta|$. Polynomial expansions in terms of δ/R_γ necessarily fail to capture this limit. From the Young-Laplace equation, it follows that

$$\frac{dR_\gamma}{d\varphi} = \frac{1}{\varphi}\frac{d\gamma}{d\varphi} - \frac{\gamma}{\varphi^2}, \tag{28}$$

while the reduced length scale appearing in the Tolman equation can be transformed to

$$\frac{\delta}{R_\gamma} = \frac{\eta\varphi + \gamma_\infty}{\gamma} - 1, \tag{29}$$

by using Eqs. (1), (4), (8), and (11). The Tolman relation can thus be converted to

$$\begin{aligned}\frac{d\gamma}{d\varphi} &= -\frac{2\gamma}{\varphi}\left(\frac{\delta}{R_\gamma} + \left[\frac{\delta}{R_\gamma}\right]^2 + \frac{1}{3}\left[\frac{\delta}{R_\gamma}\right]^3\right) \\ &= \frac{2\gamma}{3\varphi}\left(1 - \left[\frac{\eta\varphi + \gamma_\infty}{\gamma}\right]^3\right).\end{aligned} \tag{30}$$

This representation of the Tolman expression is fully equivalent to Eq. (9).

For $\varphi \to 0$, further considerations are required. There, the curvature dependence of γ as specified by Eq. (30) is self-consistent only under an additional condition. To demonstrate this, it is helpful to consider the exact Tolman equation in a different form:

$$\frac{d\gamma}{d\varphi} = \frac{2}{\gamma^2}\left(\frac{1}{3}[\zeta - \eta^3\varphi^2] - \gamma_\infty\eta[\gamma_\infty + \eta\varphi]\right). \tag{31}$$

This is obtained from Eq. (30) by expanding the cubic term. Therein, ζ has been defined as

$$\zeta = \frac{\gamma^3 - \gamma_\infty^3}{\varphi}. \tag{32}$$

For the sake of conciseness, the notation

$$q_\infty^{(i)} = \lim_{\varphi\to 0}\frac{d^i q}{d\varphi^i} \tag{33}$$

is used here for the ith derivative of a quantity q in the zero-curvature limit. The slope of γ can be obtained by inserting

$$\zeta_\infty = [\gamma^3]'_\infty = 3\gamma_\infty^2\gamma'_\infty \tag{34}$$

into Eq. (31), which yields

$$\gamma'_\infty = 2\eta_\infty. \tag{35}$$

Expanding the excess equimolar radius as

$$\eta = \eta_\infty + \eta'_\infty\varphi + O(\varphi^2) \tag{36}$$

and inserting this expression as well as Eq. (35) into the planar limit of Eq. (31) leads to

$$[\gamma^3]''_\infty = 12\gamma_\infty\eta_\infty^2 \tag{37}$$

and

$$\gamma_\infty\gamma''_\infty = -4\eta_\infty^2. \tag{38}$$

By considering the zero-curvature limit for the third derivative of γ^3, a theorem for the slope of η can now be deduced. Based on Eqs. (34) and (37), a Taylor expansion for $d(\gamma^3)/d\varphi$ in terms of φ,

$$\frac{d}{d\varphi}\gamma^3 = [\gamma^3]'_\infty + [\gamma^3]''_\infty\varphi + \frac{1}{2}[\gamma^3]'''_\infty\varphi^2 + O(\varphi^3), \quad (39)$$

yields

$$\zeta = \frac{1}{\varphi}\int_0^\varphi d\varphi \left(\frac{d}{d\varphi}\gamma^3\right) = 6\gamma_\infty^2\eta_\infty + 6\gamma_\infty\eta_\infty^2\varphi + \frac{\varphi^2}{6}[\gamma^3]'''_\infty + O(\varphi^3). \quad (40)$$

From Eqs. (35)–(40),

$$6\gamma_\infty\left(\gamma_\infty\eta'_\infty + \eta_\infty^2\right) + \frac{\varphi}{6}[\gamma^3]'''_\infty = 0 + O(\varphi) \quad (41)$$

follows by applying the full Tolman equation [cf. Eq. (31)] in the planar limit. However, this implies

$$\eta'_\infty = -\frac{\eta_\infty^2}{\gamma_\infty}, \quad (42)$$

which constitutes a necessary boundary condition for the Tolman approach in terms of η and φ.

Thus, while there is a direct correspondence between δ_∞ and η_∞, no such relation exists in the case of δ'_∞ and η'_∞, i.e., their respective derivatives (in terms of φ) in the zero-curvature limit; instead, η'_∞ is fully determined by η_∞ and thus by δ_∞, the Tolman length of the planar interface. This means that data for the excess equimolar radius for large radii have a double significance regarding the planar limit: On the one hand, they can be extrapolated to $\varphi = 0$, leading to an estimate for the planar Tolman length and the curvature dependence of γ to first order in terms of φ or $1/R_\gamma$; on the other hand, the slope of η is in itself relevant, since its zero-curvature limit η'_∞ also provides information on η_∞.

The equivalent of the exact Tolman equation in terms of the excess equimolar radius η and the pressure difference characterized by φ is Eq. (30). An expansion as a power series, analogous to Eq. (10), can be obtained as

$$\gamma = \gamma_\infty + 2\eta_\infty\varphi - \frac{2\eta_\infty^2}{\gamma_\infty}\varphi^2 + O(\varphi^3). \quad (43)$$

The planar limit, where higher-order terms can be neglected, can be treated accurately with expressions like Eq. (43). Away from the planar limit, Eq. (30) applies without any further condition (since the boundary condition for the slope of η is relevant only for $\varphi \to 0$), while Eq. (43) becomes an approximation.

IV. THE EXCESS EQUIMOLAR RADIUS FROM MOLECULAR SIMULATION

With the MARDYN MD program, developed by Bernreuther and co-workers [65–67], the canonical ensemble is simulated for small systems, corresponding to equilibrium conditions for nanoscopic liquid drops surrounded by supersaturated vapor. The TSLJ pair potential

$$u(r) = \begin{cases} 4\varepsilon\left[\left(\frac{\sigma}{r}\right)^{12} - \left(\frac{\sigma}{r}\right)^{6}\right] + u_{\text{shift}} & \text{for} \quad r < r_c, \\ 0 & \text{for} \quad r \geqslant r_c, \end{cases} \quad (44)$$

with the size parameter σ, the energy parameter ε, and a cutoff at $r_c = 2.5\sigma$ is employed as a fluid model here, including a shift by $u_{\text{shift}} = 4\varepsilon[(\sigma/r_c)^6 - (\sigma/r_c)^{12}]$ to make the potential continuous. The TSLJ model is an adequate basis for the investigation of bulk and interfacial properties of simple spherical conformal fluids (e.g., noble gases and methane) at the molecular level; cf. Vrabec *et al.* [27]. On account of this, numerous studies on nanoscopic TSLJ liquid drops have been reported [19,26,27,68–72]. The TSLJ fluid can thus be regarded as a key benchmark for theoretical and simulation approaches to the problem of curved vapor-liquid interfaces.

Certain of the general properties of this simple model, taking only short-range interactions into account, can be assumed to carry over to polar fluids as well [73], except for temperatures in the vicinity of the critical point. It is clear, however, that a qualitatively different behavior is expected for the liquid drops formed by water with and without ionic species [74,75], liquid crystals [76], and similar complex fluids. Such systems are beyond the scope of the present study.

Liquid drops are investigated at reduced temperatures between $kT/\varepsilon = 0.65$ and 0.95, covering most of the range between the triple-point temperature (which is ≈0.55 according to Bolhuis and Chandler [77], ≈0.618 as determined by Toxværd [78], and ≈0.65 according to van Meel *et al.* [70]) and the critical temperature, which several independent studies have consistently obtained as 1.08 for the TSLJ fluid [27,79,80]. The Verlet leapfrog algorithm is employed to solve the classical equations of motion numerically with an integration time step of 0.002 in Lennard-Jones (LJ) time units, i.e., $\sigma\sqrt{m/\varepsilon}$, where m is the mass of a particle. Cubic simulation volumes with 290–126 000 particles, applying the periodic boundary condition, are equilibrated for at least 2000 time units. Subsequently, spherically averaged density profiles $\rho(z)$, with their origin ($z = 0$) at the center of mass of the whole system, are constructed with a binning scheme based on equal volume concentric spheres using sampling intervals between 1000 and 40 000 time units, depending on the total simulation time, to gather multiple samples for each system. Examples of the density profiles obtained with this method are shown in Figs. 2–4.

The density profiles of TSLJ vapor-liquid interfaces are known to agree well with an expression based on two hyperbolic tangent terms, to which $\rho(z)$ has been successfully correlated for liquid drops by Vrabec *et al.* [27]. The present method merely requires the bulk densities ρ^ℓ and ρ^v corresponding to a certain value of μ or φ, which are determined here by correlating the outer parts of the density profile and extrapolating them to regions far from the interface. The densities of the coexisting fluid phases are thus deduced from the simulated profiles by correlating the exponential terms

$$\rho^\ell = \rho(z) + \alpha^\ell \exp(\beta^\ell[z - z^\ell]), \qquad \rho^v = \rho(z) - \alpha^v \exp(\beta^v[z^v - z]), \quad (45)$$

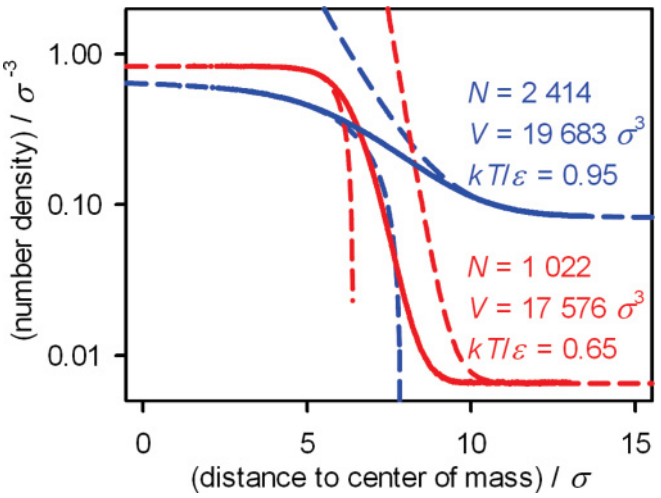

FIG. 2. (Color online) Density profiles from canonical MD simulations of TSLJ liquid drops at the reduced temperatures of $kT/\varepsilon = 0.65$ and 0.95, showing the average densities from simulation (•) and exponential approximants (– –). The steeper profile corresponds to the lower temperature.

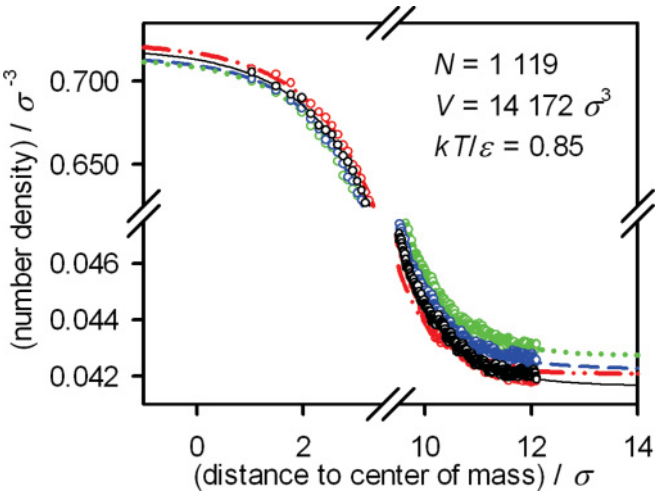

FIG. 4. (Color) Density profiles from a single canonical MD simulation of a TSLJ liquid drop, showing the average densities from simulation (○) and exponential approximants (curves) corresponding to the sampling intervals 2000–3000 (· · ·; green), 3000–4000 (·–·; red), 4000–5000 (—·-; blue), and 5000–6000 time units (—; black) after the onset of the simulation. The standard deviation between the densities at an infinite distance from the interface, according to the exponential fits for all sampling intervals of a single MD simulation, is used to determine the error of the bulk densities here.

to the data for the inner- and outermost spherical bins of the density profiles; cf. Fig. 2. These terms, which are based on those employed by Lekner and Henderson [63], asymptotically agree with the hyperbolic tangent expression of Vrabec *et al.* [27]. From the liquid and vapor densities ρ^ℓ and ρ^v obtained from the fit to Eq. (45), the equimolar radius R_ρ is calculated according to Eq. (3). The respective margins of error are obtained as standard deviations from the profiles belonging to different sampling intervals of the same MD simulation (cf. Fig. 4), of which there are at least three in all cases. The corresponding pressures P^ℓ and P^v are computed from canonical MD simulation of the bulk fluid at the respective densities; see Table I.

For the surface tension in the zero-curvature limit (as a function of the reduced temperature), the values $\gamma_\infty(0.65) = (0.680 \pm 0.009)\varepsilon\sigma^{-2}$, $\gamma_\infty(0.75) = (0.493 \pm 0.008)\varepsilon\sigma^{-2}$, $\gamma_\infty(0.85) = (0.317 \pm 0.007)\varepsilon\sigma^{-2}$, and $\gamma_\infty(0.95) = (0.158 \pm 0.006)\varepsilon\sigma^{-2}$ are taken from the correlation of Vrabec *et al.* [27]; the error corresponds to the individual data points for γ_∞ from the same source. In the case of $kT/\varepsilon = 0.9$, the higher precision of the computations by van Giessen and Blokhuis is exploited, using the value $\gamma_\infty = (0.227 \pm 0.002)\varepsilon\sigma^{-2}$ obtained from a linear fit to data for the curved interface; cf. Fig. 1. The assumption made for the error is rather generous in this case, considering that the agreement between the individual data points for φR_ρ suggests an even higher precision.

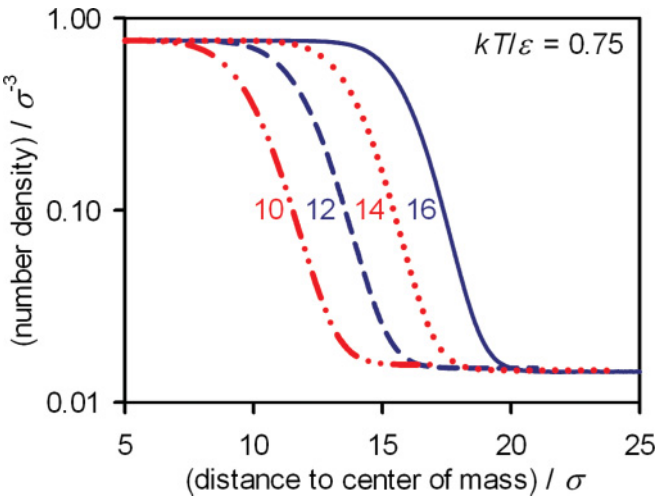

FIG. 3. (Color online) Density profiles from canonical MD simulations of TSLJ liquid drops at $kT/\varepsilon = 0.75$ with equimolar radii of $R_\rho = 9.977 \pm 0.001$ (·—·), 12.029 ± 0.003(– –),$13.974 \pm 0.002\sigma$ (· · ·) and $15.967 \pm 0.001\sigma$ (—); cf. Tables II and III.

Combining these quantities provides values for the capillarity radius R_κ and the excess equimolar radius η. Note that the margin of error for η, as indicated in Table II, contains contributions quantifying the accuracy of γ_∞ and the precision of the MD simulations of the liquid drop itself as well as those of the homogeneous vapor and liquid phases. While the vapor pressure P^v and the equimolar radius R_ρ are obtained with a high precision, the liquid pressure and the surface tension in the zero-curvature limit are major sources of uncertainty here. In both cases, methodical changes can be expected to increase the precision significantly: regarding γ_∞, it can be seen from Fig. 1 that it is now possible to reach a level of confidence beyond that of the data of Vrabec *et al.* [27] which are also examined here. For the pressure of the liquid P^ℓ, approaches based on the chemical potential, which can be determined in any region of the simulation volume (including the vapor phase), are expected to lead to significant improvements in combination with a reliable equation of state or high-precision simulations in the grand canonical ensemble.

A full summary of the simulation results where η could be determined with error bars smaller than σ is given in Table III. Note that to achieve full consistency with the Tolman approach,

TABLE I. Bulk pressure P from canonical MD simulation of (homogeneous) vapor and liquid states of the TSLJ fluid at a specified reduced temperature kT/ε and density ρ. All values are given in LJ units, and the error in terms of the last digit is specified in parentheses.

kT/ε	ρ (units of σ^{-3})	P (units of $\varepsilon\sigma^{-3}$)	kT/ε	ρ (units of σ^{-3})	P (units of $\varepsilon\sigma^{-3}$)
0.65	0.00651	0.00396(1)	0.65	0.8298	0.220(8)
0.65	0.00904	0.005371(5)	0.65	0.8567	0.65(1)
0.75	0.01340	0.00907(3)	0.75	0.76434	0.04(1)
0.75	0.01381	0.00932(4)	0.75	0.76492	0.05(2)
0.75	0.01401	0.00944(2)	0.75	0.76532	0.05(1)
0.75	0.01405	0.00946(1)	0.75	0.76723	0.0686(6)
0.75	0.01442	0.009690(4)	0.75	0.76733	0.0695(4)
0.75	0.01442	0.00968(3)	0.75	0.76835	0.075(9)
0.75	0.01451	0.009743(7)	0.75	0.7679	0.0746(4)
0.75	0.01469	0.009848(5)	0.75	0.76853	0.0799(8)
0.75	0.01506	0.010065(6)	0.75	0.76968	0.0904(3)
0.75	0.01556	0.01035(1)	0.75	0.7703	0.0958(5)
0.75	0.01566	0.01042(1)	0.75	0.77212	0.1125(5)
0.75	0.01676	0.01104(2)	0.75	0.7753	0.140(7)
0.75	0.01731	0.01135(1)	0.75	0.7774	0.1626(5)
0.75	0.02136	0.01354(5)	0.75	0.8109	0.55(1)
0.85	0.03708	0.02492(4)	0.85	0.7135	0.097(1)
0.85	0.04211	0.0273(1)	0.85	0.733	0.23(1)
0.9	0.05041	0.03396(2)	0.9	0.67379	0.0671(4)
0.9	0.05315	0.03516(2)	0.9	0.67734	0.0820(1)
0.9	0.05731	0.03688(4)	0.9	0.6868	0.1252(5)
0.95	0.08249	0.0503(2)	0.95	0.6615	0.169(9)

the bulk densities ρ^ℓ and ρ^v from Eq. (45) have to match those of the bulk fluid at the same temperature and chemical potential as the two-phase system. Regarding liquid drops with $R_\rho > 8\ \sigma$, this is certainly the case, since constant-density regions of the profile in the liquid and vapor regions are actually present; cf. Fig. 3. However, the values determined for the smallest drops here rely on the validity of the correlation given by Eq. (45) and can be considered valid only as far as this expression itself does not introduce any major deviations, an assumption that remains open to further examination; a version

TABLE II. Error analysis for the excess equimolar radius η of TSLJ liquid drops at the reduced temperature of $kT/\varepsilon = 0.75$. The number of particles N, the volume V of the periodic simulation box, and the total simulation time t for simulations of the liquid drops are indicated alongside the contributions to the uncertainty of η from the pressure P^ℓ of the liquid phase (determined by canonical MD simulation of the bulk liquid), the surface tension γ_∞ of the planar vapor-liquid interface (cf. Vrabec *et al.* [27]), the vapor pressure P^v (obtained in an analogous manner to P^ℓ), and the equimolar radius R_ρ (from the density profiles of the liquid drops). Note that the time unit, i.e., $\sigma\sqrt{m/\varepsilon}$, corresponds to 500 simulation time steps here. The flat symbols (♭) indicate the fraction of the margin of error for η due to the respective quantities. All values are given in LJ units, and the error in terms of the last digit is specified in parentheses. In the subsequent discussion, the cases where the uncertainty of η exceeds 1σ are disregarded.

N	V (units of σ^{-3})	t (units of $\sigma\sqrt{m/\varepsilon}$)	P^ℓ (units of $\varepsilon\sigma^{-3}$)	♭ P^ℓ	♭ γ_∞	P^v (units of $\varepsilon\sigma^{-3}$)	♭ P^v	R_ρ (units of σ)	♭ R_ρ	η (units ofσ)
497	10648	60000	0.6(1)	84%	5.9%	0.0135(3)	0.23%	4.33(5)	9.5%	2.5(5)
1418	21952	48176	0.16(1)	82%	17%	0.01136(5)	0.37%	6.883(3)	0.5%	0.4(6)
1766	21952	6000	0.14(3)	94%	5.3%	0.0110(2)	0.58%	7.61(1)	0.55%	0(2)
3762	39304	221244	0.113(2)	53%	45%	0.01042(4)	1.0%	9.977(1)	0.28%	0.3(3)
5161	54872	64219	0.096(3)	63%	34%	0.0104(1)	2.4%	11.089(4)	0.82%	−0.4(5)
6619	74088	162678	0.090(2)	59%	40%	0.01007(2)	0.75%	12.029(3)	0.57%	−0.2(5)
10241	110592	185460	0.080(1)	56%	43%	0.00985(2)	0.58%	13.974(2)	0.29%	−0.1(5)
12651	140608	32594	0.075(2)	66%	32%	0.00974(4)	1.2%	14.981(6)	0.78%	−0.2(8)
15237	166375	135348	0.070(2)	66%	33%	0.00969(1)	0.35%	15.967(1)	0.15%	−0.5(8)
17113	169418	6006	0.08(1)	89%	9.8%	0.00969(9)	0.78%	16.689(4)	0.18%	2(2)
24886	238328	27272	0.069(9)	90%	9.7%	0.00947(3)	0.3%	18.969(5)	0.17%	2(3)
28327	238328	6006	0.056(9)	92%	7.5%	0.00945(3)	0.28%	19.950(8)	0.18%	−1(5)
38753	247673	6000	0.050(7)	90%	8.8%	0.00932(5)	0.69%	22.391(7)	0.15%	−2(4)
125552	697078	6006	0.042(5)	89%	9.6%	0.00908(9)	1.6%	33.31(1)	0.21%	3(5)

TABLE III. Number of particles N, volume V of the simulation box, and reduced temperature kT/ε of the canonical simulations of TSLJ liquid drops surrounded by vapor, together with the main results from the spherical density profiles, i.e., the equimolar radius R_ρ and the densities ρ^ℓ and ρ^v. For drop radii above 8σ, these values can be reliably regarded as identical with those corresponding to the present theoretical approach, which is highlighted with the bold typeface. In the cases of smaller radii (italic typeface), inaccuracies can arise due to the application of exponential approximants for the density profiles; cf. Fig. 2 and Eq. (45). Results from MD simulation of the bulk fluid (cf. Table I) are evaluated to obtain the corresponding pressures P^ℓ and P^v as well as the capillarity radius R_κ, and the excess equimolar radius η. All values are given in LJ units, and the error in terms of the last digit is specified in parentheses. The margin of error specified for the pressure values here is larger than in Table I, because it also contains a contribution due to the uncertainty in the density.

N	V (units of σ^3)	kT/ε	ρ^ℓ (units of σ^{-3})	ρ^v (units of σ^{-3})	P^ℓ (units of $\varepsilon\sigma^{-3}$)	P^v (units of $\varepsilon\sigma^{-3}$)	R_κ (units of σ)	R_ρ (units of σ)	η (units of σ)
291	8999	0.65	*0.857(5)*	*0.0090(2)*	*0.65(8)*	*0.0054(1)*	*2.1(3)*	*3.90(1)*	*1.8(3)*
1022	17576	0.65	*0.830(1)*	*0.00651(7)*	*0.22(2)*	*0.00397(4)*	*6.3(6)*	*6.407(2)*	*0.1(6)*
497	10648	0.75	*0.81(1)*	*0.0214(6)*	*0.6(1)*	*0.0135(4)*	*1.8(5)*	*4.33(5)*	*2.5(5)*
1418	21952	0.75	*0.777(1)*	*0.0173(1)*	*0.16(1)*	*0.01136(5)*	*6.5(6)*	*6.883(3)*	*0.4(6)*
3762	39304	0.75	**0.7721(2)**	**0.01566(6)**	**0.113(2)**	**0.01042(4)**	**9.7(4)**	**9.977(1)**	**0.3(4)**
5161	54872	0.75	**0.7703(2)**	**0.0156(2)**	**0.096(3)**	**0.0104(1)**	**11.5(5)**	**11.089(4)**	**−0.5(6)**
6619	74088	0.75	**0.7697(2)**	**0.01506(4)**	**0.090(2)**	**0.01007(2)**	**12.3(5)**	**12.029(3)**	**−0.2(5)**
10241	110592	0.75	**0.7685(1)**	**0.01469(3)**	**0.080(2)**	**0.00985(2)**	**14.1(5)**	**13.974(2)**	**−0.1(5)**
12651	140608	0.75	**0.7679(2)**	**0.01451(7)**	**0.075(2)**	**0.00974(4)**	**15.2(8)**	**14.981(6)**	**−0.2(8)**
15237	166375	0.75	**0.7673(2)**	**0.01442(2)**	**0.070(2)**	**0.00969(1)**	**16.5(8)**	**15.967(1)**	**−0.5(8)**
1119	14172	0.85	*0.733(7)*	*0.0421(5)*	*0.23(5)*	*0.0273(2)*	*3.1(9)*	*6.79(6)*	*2.5(9)*
3357	32768	0.85	**0.7135(8)**	**0.0371(5)**	**0.097(5)**	**0.0249(2)**	**8.8(8)**	**9.11(1)**	**0.4(9)**
2031	21952	0.9	*0.687(3)*	*0.0573(8)*	*0.13(1)*	*0.0369(3)*	*5.1(8)*	*6.79(6)*	*1.7(9)*
4273	29791	0.9	**0.6773(9)**	**0.0532(2)**	**0.082(4)**	**0.03516(7)**	**9.7(9)**	**10.086(9)**	**0.4(9)**
11548	85184	0.9	**0.6738(1)**	**0.0504(2)**	**0.0672(6)**	**0.03396(8)**	**13.7(4)**	**14.054(8)**	**0.4(4)**
2414	19683	0.95	*0.662(2)*	*0.0825(2)*	*0.169(7)*	*0.05032(8)*	*2.7(3)*	*6.86(3)*	*4.2(3)*

of the present method where P^ℓ is computed from μ could resolve this issue.

V. DISCUSSION

Previous authors have made qualitatively contradictory claims about the magnitude of the Tolman length as well as its sign: Tolman himself expected δ to be positive and smaller than the length scale of the dispersive interaction, a conjecture that Kirkwood and Buff [62] appeared to confirm from a statistical mechanical point of view, based on a mechanical approach. Subsequent studies, however, have also found δ to be negligible or even equal to zero [21,68,81], positive and larger than σ [27,71,82,83], or negative with $-\sigma < \delta < 0$ [23,26,84–86], while others have claimed that the sign of δ is curvature dependent [87,88]. Thereby, they have only confirmed the mutual inconsistency of their assumptions and methods, while little is truly known about δ and the dependence of the surface tension on curvature.

The approach introduced in Sec. III is strictly based on axiomatic thermodynamics and relies on the fact that $\delta_\infty = -\eta_\infty$ holds in the planar limit. From the values for η reported in bold face in Table III, corresponding to $R_\rho > 8\sigma$, the excess equimolar radius for liquid drops of the TSLJ fluid is unequivocally shown to be smaller in magnitude than $\sigma/2$, while its remains unclear whether it is positive, negative, of both signs (depending on the curvature), or equal to zero. No definite conclusion can be drawn regarding the dependence of η on curvature. Since this means that, at the present level of accuracy, no significant dependence of γ on the radius of the liquid drop could be detected, the statement of Mareschal *et al.* [89] regarding cylindrical interfaces also applies here: Considering "the large fluctuations in the bulk liquid phase [cf. the error analysis presented in Table II] we tentatively conclude that the surface tension is independent of the curvature of the liquid-vapor interface or else that this dependence is very weak."

A notion that can be definitely dismissed is that of a large and positive Tolman length (previously also reported by some of the present authors), which is obtained by following the mechanical route to the surface tension employing the IK pressure tensor [27,71,82,83]. The same deviation between the mechanical route (leading to large positive values for δ) and a thermodynamic approach (leading to $\delta < 0.5\ \sigma$) was found by Haye and Bruin [49]. As shown in Fig. 5, the previous simulation results of Vrabec *et al.* [27] are actually consistent with those from the present study if they are interpreted in terms of the radii R_κ and R_ρ. Thereby, applying the approach of Maruyama *et al.* [90], only the density profile and the pressure in the homogeneous regions inside and outside the liquid drop are taken into account, whereas the normal pressure along the interface is not considered at all.

Since the deviation between the present and previous data disappears in such a representation, the disagreement must be caused by the inadequacy of the pressure tensor (mechanical) route implemented by Thompson *et al.* [36], as pointed out by Henderson [41]. Possible sources of error in such an approach are outlined in Sec. II. Nonetheless, more detailed methodological investigations would be expedient to determine which approximations are actually responsible for major inaccuracies, and whether they can be corrected or whether the pressure tensor route to the surface tension has to be discarded altogether.

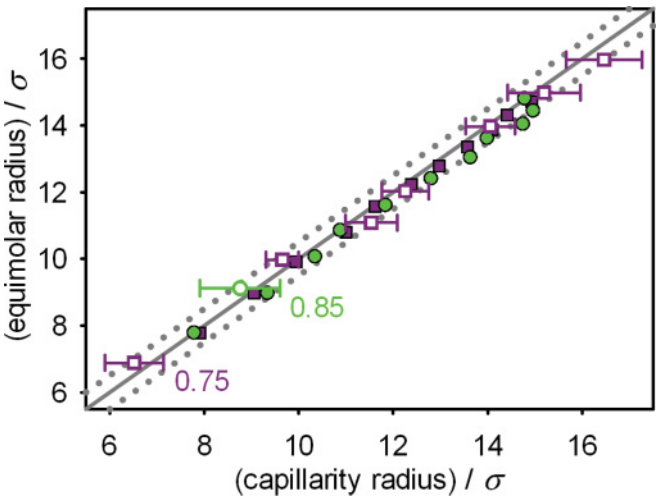

FIG. 5. (Color online) Equimolar radius R_ρ as a function of the capillarity radius R_κ for TSLJ liquid drops, from density profiles and bulk pressures determined with canonical MD simulations at reduced temperatures of $kT/\varepsilon = 0.75$ (□) and 0.85 (○), in comparison with results from the previous work of Vrabec *et al.* [27] at $kT/\varepsilon = 0.75$ (■) and 0.85 (●), using pressure differences based on evaluating the IK tensor in the (approximately) homogeneous regions inside and outside the liquid drop. The continuous diagonal line denotes $R_\rho = R_\kappa$ and thus corresponds to an excess equimolar radius of $\eta = 0$, while the dotted lines correspond to $\eta = \pm 0.5\sigma$.

ACKNOWLEDGMENTS

G.J. and E.A.M. are grateful to the Engineering and Physical Sciences Research Council (EPSRC) of the UK (Grants No. GR/T17595, No. GR/N35991, and No. EP/E016340), the Joint Research Equipment Initiative (Grant No. GR/M94427), and the Royal Society–Wolfson Foundation refurbishment scheme for funding to the Molecular Systems Engineering Group. H.H. and M.H. acknowledge support from the German Research Foundation (DFG) within the collaborative research center (SFB) 926 on "microscale morphology of component surfaces" (MICOS) as well as the Boltzmann-Zuse Society of Computational Molecular Engineering (BZS), and M.H. was supported at Imperial College London by a fellowship within the postdoctoral program of the German Academic Exchange Service (DAAD). The computations were performed on the NEC Nehalem cluster "laki" at the High Performance Computing Center Stuttgart (HLRS) with resources allocated according to the grant MMHBF. Furthermore, the authors would like to thank D. Reguera López and J. Wedekind (Barcelona), F. Römer (London), M. Schrader (Mainz), A. Bedhotiya (Mumbai), Z. Lin, S. K. Miroshnichenko, S. Olma, and Z. Wei (Paderborn), D. V. Tatyanenko (St. Petersburg), and M. F. Bernreuther, S. Dietrich, C. W. Glass, S. Grottel, C. Niethammer, and G. Reina (Stuttgart) for contributing to various theoretical and practical issues through helpful suggestions and their participation in relevant discussions or by assisting at the debugging process.

[1] T. Young, Philos. Trans. R. Soc. London **95**, 65 (1805).
[2] P.-S. de Laplace, *Traité de Méchanique Céleste* (Bachelier, Paris, 1806), Vol. 3.
[3] J. S. Rowlinson and B. Widom, *Molecular Theory of Capillarity* (Clarendon Press, Oxford, 1982).
[4] J. W. Gibbs, Trans. Connecticut Acad. Arts Sci. **3**, 108 (1878).
[5] J. W. Gibbs, Am. J. Sci. (Ser. 3) **16**, 441 (1878).
[6] M. Volmer and A. Weber, Z. Phys. Chem. **119**, 277 (1926).
[7] L. Farkas, Z. Phys. Chem. **125**, 236 (1927).
[8] R. Becker and W. Döring, Ann. Phys. (Leipzig) **24**, 719 (1935).
[9] F. Kuhrt, Z. Phys. **131**, 185 (1952).
[10] J. Feder, K. C. Russell, J. Lothe and G. M. Pound, Adv. Phys. **15**, 111 (1966).
[11] R. H. Weber, Ann. Phys. (Leipzig) **4**, 706 (1901).
[12] F. P. Buff, J. Chem. Phys. **19**, 1591 (1951).
[13] F. P. Buff, J. Chem. Phys. **23**, 419 (1955).
[14] S. Kondo, J. Chem. Phys. **25**, 662 (1956).
[15] R. C. Tolman, J. Chem. Phys. **16**, 758 (1948).
[16] R. C. Tolman, J. Chem. Phys. **17**, 118 (1949).
[17] R. C. Tolman, J. Chem. Phys. **17**, 333 (1949).
[18] A. J. Castellanos Suárez, J. Toro Mendoza and M. García Sucre, J. Phys. Chem. B **133**, 5981 (2009).
[19] B. J. Block, S. K. Das, M. Oettel, P. Virnau and K. Binder, J. Chem. Phys. **133**, 154702 (2010).
[20] S. K. Das and K. Binder, Phys. Rev. E **84**, 061607 (2011).
[21] T. Bieker and S. Dietrich, Physica A **252**, 85 (1998); **259**, 466 (1998).
[22] M. Schrader, P. Virnau, D. Winter, T. Zykova-Timan, and K. Binder, Eur. Phys. J. Spec. Top. **177**, 103 (2009).
[23] J. G. Sampayo, A. Malijevský, E. A. Müller, E. de Miguel, and G. Jackson, J. Chem. Phys. **132**, 141101 (2010).
[24] A. Malijevský and G. Jackson (unpublished).
[25] M. J. P. Nijmeijer, C. Bruin, A. B. van Woerkom, A. F. Bakker, and J. M. J. van Leeuwen, J. Chem. Phys. **96**, 565 (1991).
[26] A. E. van Giessen and E. M. Blokhuis, J. Chem. Phys. **131**, 164705 (2009).
[27] J. Vrabec, G. K. Kedia, G. Fuchs, and H. Hasse, Mol. Phys. **104**, 1509 (2006).
[28] P. R. ten Wolde and D. Frenkel, J. Chem. Phys. **109**, 9901 (1998).
[29] H. Matsubara, T. Koishi, T. Ebisuzaki, and K. Yasuoka, J. Chem. Phys. **127**, 214507 (2007).
[30] J. Vrabec, M. Horsch, and H. Hasse, J. Heat Transfer **131**, 043202 (2009).
[31] Z.-Y. Hou, L.-X. Liu, R.-S. Liu, Z.-A. Tian, and J.-G. Wang, Chem. Phys. Lett. **491**, 172 (2010).
[32] G. Chkonia, J. Wölk, R. Strey, J. Wedekind, and D. Reguera, J. Chem. Phys. **130**, 064505 (2009).
[33] M. P. A. Fisher and M. Wortis, Phys. Rev. B **29**, 6252 (1984).
[34] E. M. Blokhuis and D. Bedeaux, Mol. Phys. **80**, 705 (1993).
[35] T. V. Bykov and A. K. Shchekin, Inorg. Mater. **35**, 641 (1999).

[36] S. M. Thompson, K. E. Gubbins, J. P. R. B. Walton, R. A. R. Chantry, and J. S. Rowlinson, J. Chem. Phys. **81**, 530 (1984).
[37] M. Schrader, P. Virnau, and K. Binder, Phys. Rev. E **79**, 061104 (2009).
[38] G. J. Gloor, G. Jackson, F. J. Blas, and E. de Miguel, J. Chem. Phys. **123**, 134703 (2005).
[39] A. Ghoufi, F. Goujon, V. Lachet, and P. Malfreyt, Phys. Rev. E **77**, 031601 (2008).
[40] A. Ghoufi and P. Malfreyt, J. Chem. Phys. **135**, 104105 (2011).
[41] J. R. Henderson, in *Fluid Interfacial Phenomena*, edited by C. A. Croxton (Wiley, New York, 1986), pp. 555–605.
[42] G. Bakker, *Kapillarität und Oberflächenspannung*, Handbuch der Experimentalphysik No. 6 (Akademische Verlagsgesellschaft, Leipzig, 1928).
[43] A. Harasima, J. Phys. Soc. Jpn. **8**, 343 (1953).
[44] V. G. Baidakov and G. S. Boltachev, Phys. Rev. E **59**, 469 (1999).
[45] J. H. Irving and J. G. Kirkwood, J. Chem. Phys. **18**, 817 (1950).
[46] E. M. Blokhuis and D. Bedeaux, J. Chem. Phys. **97**, 3576 (1992).
[47] J. R. Henderson and J. Lekner, Mol. Phys. **36**, 781 (1978).
[48] K. Binder, Phys. Rev. A **25**, 1699 (1982).
[49] M. J. Haye and C. Bruin, J. Chem. Phys. **100**, 556 (1994).
[50] J. P. R. B. Walton, D. J. Tildesley, J. S. Rowlinson, and J. R. Henderson, Mol. Phys. **48**, 1357 (1983).
[51] P. Schofield and J. R. Henderson, Proc. R. Soc. London, Ser. A **379**, 231 (1982).
[52] G. M. Torrie and J. P. Valleau, J. Comput. Phys. **23**, 187 (1977).
[53] P. Virnau and M. Müller, J. Chem. Phys. **120**, 10925 (2004).
[54] A. Tröster and K. Binder, Phys. Rev. Lett. **107**, 265701 (2011).
[55] M. J. McGrath, J. N. Ghogomu, N. T. Tsona, J. I. Siepmann, B. Chen, I. Napari, and H. Vehkamäki, J. Chem. Phys. **133**, 084106 (2010).
[56] R. B. Nellas, S. J. Keasler, J. I. Siepmann, and B. Chen, J. Chem. Phys. **132**, 164517 (2010).
[57] C. H. Bennett, J. Comput. Phys. **22**, 245 (1976).
[58] R. W. Zwanzig, J. Chem. Phys. **22**, 1420 (1954).
[59] B. Widom, J. Chem. Phys. **39**, 2808 (1963).
[60] F. J. Blas, L. G. MacDowell, E. de Miguel, and G. Jackson, J. Chem. Phys. **129**, 144703 (2008).
[61] J. G. Sampayo Hernández, Ph.D. thesis, Department of Chemical Engineering, Imperial College London, 2010.
[62] J. G. Kirkwood and F. P. Buff, J. Chem. Phys. **17**, 338 (1949).
[63] J. Lekner and J. R. Henderson, Mol. Phys. **34**, 333 (1977).
[64] J. K. Percus, L. A. Pozhar, and K. E. Gubbins, Phys. Rev. E **51**, 261 (1995).
[65] M. Bernreuther and J. Vrabec, in *High Performance Computing on Vector Systems*, edited by M. Resch, T. Bönisch, K. Benkert, T. Furui, and W. Bez (Springer, Heidelberg, 2006), pp. 187–195.
[66] M. Bernreuther, C. Niethammer, M. Horsch, J. Vrabec, S. Deublein, H. Hasse, and M. Buchholz, Innovatives Supercomputing in Deutschland **7**, 50 (2009).
[67] M. Buchholz, H.-J. Bungartz, and J. Vrabec, J. Comput. Sci. **2**, 124 (2011).
[68] Y. A. Lei, T. Bykov, S. Yoo, and X. C. Zeng, J. Am. Chem. Soc. **127**, 15346 (2005).
[69] R. Hołyst and M. Litniewski, Phys. Rev. Lett. **100**, 055701 (2008).
[70] J. A. van Meel, A. J. Page, R. P. Sear, and D. Frenkel, J. Chem. Phys. **129**, 204505 (2008).
[71] M. Horsch, J. Vrabec, and H. Hasse, Phys. Rev. E **78**, 011603 (2008).
[72] I. Napari, J. Julin, and H. Vehkamäki, J. Chem. Phys. **133**, 154503 (2010).
[73] I. Nezbeda, Mol. Phys. **103**, 59 (2005).
[74] R. G. Harrison and M. H. P. Ambaum, Proc. R. Soc. London, Ser. A **464**, 2561 (2008).
[75] N. Galamba, J. Chem. Phys. **133**, 124510 (2010).
[76] M. Houssa, L. F. Rull, and J. M. Romero Enrique, J. Chem. Phys. **130**, 154504 (2009).
[77] P. G. Bolhuis and D. Chandler, J. Chem. Phys. **113**, 8154 (2000).
[78] S. Toxværd, J. Phys. Chem. C **111**, 15620 (2007).
[79] W. Shi and J. K. Johnson, Fluid Phase Equilib. **187–188**, 171 (2001).
[80] B. Smit, J. Chem. Phys. **96**, 8639 (2002).
[81] D. Zhou, M. Zeng, J. Mi, and C. Zhong, J. Phys. Chem. B **115**, 57 (2011).
[82] H. Yaguchi, T. Yano, and S. Fujikawa, J. Fluid Sci. Technol. **5**, 180 (2010).
[83] R.-Z. Zhu and H. Yan, Chin. Phys. B **20**, 016801 (2011).
[84] S. J. Hemingway, J. R. Henderson, and J. S. Rowlinson, Faraday Symp. Chem. Soc. **16**, 33 (1981).
[85] A. E. van Giessen, E. M. Blokhuis, and D. J. Bukman, J. Chem. Phys. **108**, 1148 (1998).
[86] P. Bryk, R. Roth, K. R. Mecke, and S. Dietrich, Phys. Rev. E **68**, 031602 (2003).
[87] K. Koga, X. C. Zeng, and A. K. Shchekin, J. Chem. Phys. **109**, 4063 (1998).
[88] J. Julin, I. Napari, J. Merikanto, and H. Vehkamäki, J. Chem. Phys. **133**, 044704 (2010).
[89] M. Mareschal, M. Baus, and R. Lovett, J. Chem. Phys. **106**, 645 (1997).
[90] S. Maruyama, S. Matsumoto, M. Shoji, and A. Ogita, in *Proceedings of the X. International Heat Transfer Conference (Heat Transfer 1994)*, edited by G. F. Hewitt (Institute of Chemical Engineers, Rugby, Warwickshire, 1994), Vol. 2, pp. 409–414.